

# The Organism/Organic Exposure to Orbital Stresses (O/OREOS) Satellite: Radiation Exposure in Low-Earth Orbit and Supporting Laboratory Studies of Iron Tetrphenylporphyrin Chloride

Amanda M. Cook,<sup>1</sup> Andrew L. Mattioda,<sup>1</sup> Antonio J. Ricco,<sup>1</sup> Richard C. Quinn,<sup>2</sup> Andreas Elsaesser,<sup>3</sup> Pascale Ehrenfreund,<sup>4</sup> Alessandra Ricca,<sup>2</sup> Nykola C. Jones,<sup>5</sup> and Søren V. Hoffmann<sup>5</sup>

## Abstract

We report results from the exposure of the metalloporphyrin iron tetrphenylporphyrin chloride (FeTPPCL) to the outer space environment, measured *in situ* aboard the Organism/Organic Exposure to Orbital Stresses nanosatellite. FeTPPCL was exposed for a period of 17 months (3700 h of direct solar exposure), which included broad-spectrum solar radiation ( $\sim 122$  nm to the near infrared). Motivated by the potential role of metalloporphyrins as molecular biomarkers, the exposure of thin-film samples of FeTPPCL to the space environment in low-Earth orbit was monitored *in situ* via ultraviolet/visible spectroscopy and reported telemetrically. The space data were complemented by laboratory exposure experiments that used a high-fidelity solar simulator covering the spectral range of the spaceflight measurements. We found that thin-film samples of FeTPPCL that were in contact with a humid headspace gas (0.8–2.3% relative humidity) were particularly susceptible to destruction upon irradiation, degrading up to 10 times faster than identical thin films in contact with dry headspace gases; this degradation may also be related to the presence of oxides of nitrogen in those cells. In the companion terrestrial experiments, simulated solar exposure of FeTPPCL films in contact with either Ar or CO<sub>2</sub>:O<sub>2</sub>:Ar (10:0.01:1000) headspace gas resulted in growth of a band in the films' infrared spectra at 1961 cm<sup>-1</sup>. We concluded that the most likely carriers of this band are allene (C<sub>3</sub>H<sub>4</sub>) and chloropropadiene (C<sub>3</sub>H<sub>3</sub>Cl), putative molecular fragments of the destruction of the porphyrin ring. The thin films studied in space and in solar simulator-based experiments show qualitatively similar spectral evolution as a function of contacting gaseous species but display significant differences in the time dependence of those changes. The relevance of our findings to planetary science, biomarker research, and the photostability of organic materials in astrobiologically relevant environments is discussed. Key Words: Astrobiology—Spectroscopy—Low-Earth orbit—Organic matter—UV radiation. *Astrobiology* 14, 87–101.

## 1. Introduction

METALLOPORPHYRINS play an essential role in the biochemistry of living systems, participating in electron transport (*e.g.*, cytochrome *c*), pigmentation (*e.g.*, chlorophyll), oxygen transport (*e.g.*, hemoglobin, myoglobin), and other biological functions, and are therefore excellent biomarkers. Metalloporphyrins are easily recognized via spectroscopy and are relatively stable in a variety of environments

relevant to space science (Suo *et al.*, 2007 and references therein). Although metalloporphyrins are thought to be biologically produced, they have been proposed as contributors to the diffuse interstellar bands detected ubiquitously via ultraviolet/visible (UV/vis) observations of the interstellar medium (Johnson, 2006); identification of the diffuse interstellar bands is an ongoing pursuit. Motivated by the astrobiological significance of metalloporphyrins, iron(III) tetrphenylporphyrin chloride (FeTPPCL) was exposed to the

<sup>1</sup>NASA Ames Research Center, Moffett Field, California, USA.

<sup>2</sup>SETI Institute, Mountain View, California, USA.

<sup>3</sup>Leiden University, Leiden, the Netherlands.

<sup>4</sup>Space Policy Institute, Washington, DC, USA.

<sup>5</sup>ISA, Department of Physics and Astronomy, Aarhus University, Aarhus, Denmark.

radiation environment of space aboard the Space Environment Viability of Organics (SEVO) payload of the Organism/Organic Exposure to Orbital Stresses (O/OREOS) nanosatellite.

O/OREOS is a technology demonstration mission conducted under the auspices of NASA's Astrobiology Small Payloads Program. It was launched into low-Earth orbit (LEO) in November 2010 and accommodates two astrobiology experiments, SEVO and SESLO (Space Environment Survivability of Live Organisms), each housed in a separate 10 cm cube (see Fig. 1a). Design specifications and early science reports from the mission have been published elsewhere (Nicholson *et al.*, 2011; Bramall *et al.*, 2012; Mattioda *et al.*, 2012; Ehrenfreund *et al.*, 2014).

SEVO and O/OREOS contribute to a multinational legacy of experiments designed to examine changes in organic compounds when exposed to space radiation (Kinard *et al.*, 1994; Dever *et al.*, 2008; Guan *et al.*, 2010; Bryson *et al.*, 2011, Rabbow *et al.*, 2012). However, SEVO is the first experiment with the capability to return data collected *in situ* at multiple time points over the course of months-long space exposure in LEO, rather than before the experiment is deployed in space and again after its return to Earth. (O/OREOS will not return to Earth; it will disintegrate upon atmospheric reentry in approximately 2032.) SEVO was designed to explore the photochemistry of organic molecules and biomarkers exposed to space radiation—solar exposure being the dominant factor—under different experimental conditions including variations in the partial pressure of water, headspace gas composition, contacting solid substrate composition, and spectral filtering. Mattioda *et al.* (2012) reported initial flight results for two organic samples: isoviolanthrene (a large polycyclic aromatic hydrocarbon) and anthrurufin (a quinone). This paper reports in

detail the LEO spaceflight results obtained by SEVO's compact UV/vis/NIR (near-infrared) spectrometer over a duration of 17 months ( $\sim 3700$  h of direct solar exposure) from thin-film FeTPPCL samples and includes a comparison of these results with complementary laboratory studies in which a solar simulator was used to expose samples to the  $\sim 122$ – $1000$  nm spectral range at intensities comparable to solar radiation in LEO.

## 2. Materials and Methods

### 2.1. Sample cells

Hermetically sealed sample cells (Bramall *et al.*, 2012) with controlled initial gas composition, pressure, and substrate composition were used for LEO and laboratory studies (Fig. 1b). The FeTPPCL samples were sublimed (at  $300^\circ\text{C}$ ) as thin films, 17 nm thick, directly onto  $\text{MgF}_2$  windows or on top of optically thin inorganic substrates that were pre-deposited on the  $\text{MgF}_2$  windows; sample thicknesses were measured with a quartz crystal microbalance. The structural integrity of the molecule after sublimation was verified by dissolving a subset of the sample films in dimethyl sulfoxide ( $\text{C}_2\text{H}_6\text{OS}$ ) after deposition; UV/vis spectra of the dissolved films matched that of the unheated dissolved powder sample. Spectra of cells with no organic films and spectra of “direct” solar radiation (*i.e.*, not passing through any cell prior to entering the collection optics) were used as references.

To study direct radiation-induced changes relevant to interstellar and interplanetary conditions, *Inert* sample cells contained FeTPPCL with 100 kPa argon gas. To study the effects of planetary atmospheres containing  $\text{CO}_2$ , *Atmosphere* cells contained 1 kPa  $\text{CO}_2$ , 0.001 kPa  $\text{O}_2$ , balance argon ( $\sim 100$  kPa total cell pressure) with a FeTPPCL thin

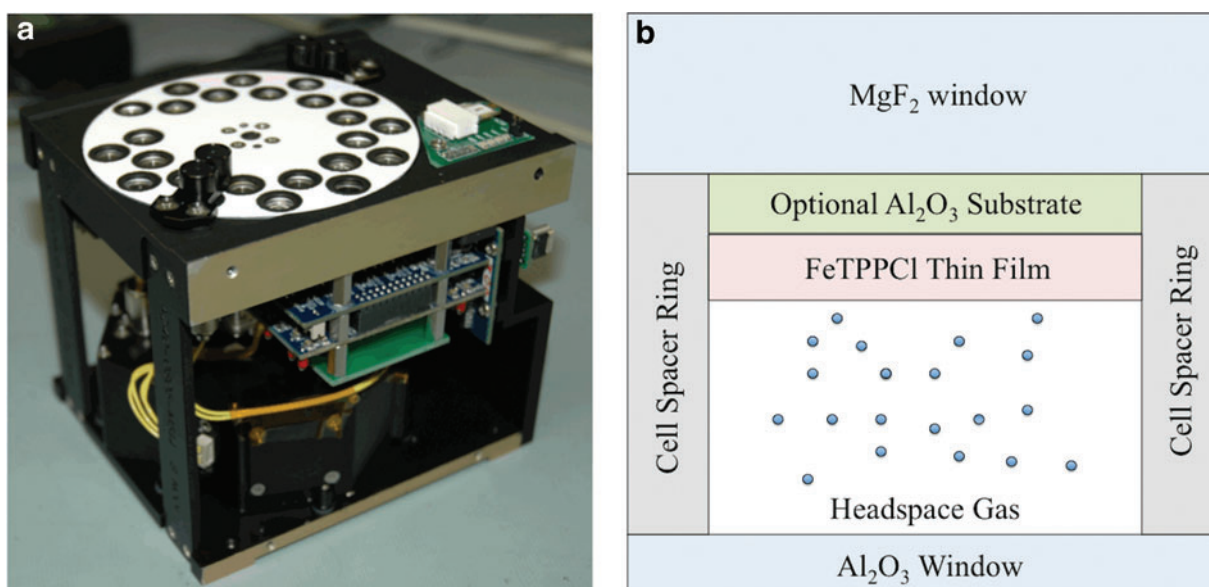


**FIG. 1.** (a) Photo of the SEVO flight module before integration onto the O/OREOS satellite. The white sample carousel is visible, with 24 positions for 18 samples, 4 microenvironment references, and 2 holes for solar reference. (b) Schematic cross section of a SEVO sample cell (not to scale). The  $\text{MgF}_2$  window is at the top of the cell; solar radiation passes through this window, then through an optional substrate film, then through the FeTPPCL thin film in contact with headspace gas, and finally through the sapphire ( $\text{Al}_2\text{O}_3$ ) window at the bottom, to be collected by an optical fiber below the cell. Color images available online at [www.liebertonline.com/ast](http://www.liebertonline.com/ast)

film deposited on top of an optically thin (200 nm) sputtered Al<sub>2</sub>O<sub>3</sub> layer supported by a MgF<sub>2</sub> substrate. The Al<sub>2</sub>O<sub>3</sub> served to filter vacuum ultraviolet (VUV) radiation (< ~170 nm) as well as provide a mineral-like surface. To study the effects of water activity, *Humid* cells contained FeTPPCL deposited on top of Al<sub>2</sub>O<sub>3</sub> (200 nm) on MgF<sub>2</sub> (here the Al<sub>2</sub>O<sub>3</sub> also protects the MgF<sub>2</sub> from degradation by water vapor). Relative humidity of 0.8–2.3% (depending upon ambient temperature, which varied from approximately –5°C to 45°C as a result of variations in the orbital solar exposure conditions) was maintained in an argon atmosphere (100 kPa) by using a hydrated salt pair supported on a stainless-steel cylindrical wire mesh located along the sidewall of each cell (out of the optical path) (Bramall *et al.*, 2012). Table 1 summarizes the conditions in each FeTPPCL cell used for both the flight experiment and supporting laboratory studies.

*5,10,15,20-Tetraphenyl-21H,23H-porphine iron(III) chloride* (FeTPPCL, ≥94% purity) was purchased from Sigma-Aldrich as a bulk powder. It was deposited as thin films (16.5 nm) onto the optical substrates (*i.e.*, MgF<sub>2</sub> or MgF<sub>2</sub> coated with 200 nm of sputtered Al<sub>2</sub>O<sub>3</sub>) by subliming the powder at ~300°C in a vacuum chamber (Bramall *et al.*, 2012).

The O/OREOS satellite was in a 72° inclination, 650 km Earth orbit, with an average rotation rate of ~1 rpm over the duration of this experiment. Satellite rotation resulted in periodic sample exposure to solar radiation for an average of 30% of the total elapsed time in space; the time-averaged net solar energy exposure flux was ~500 J/cm<sup>2</sup>/h (Ehrenfreund *et al.*, 2014), although the instantaneous flux varied significantly due to periods of solar eclipse of the spacecraft for parts of most orbits, as well as its ~1 rpm

rotation about the spacecraft's long axis. Sample spectra were collected from 200 to 1000 nm by the SEVO spectrometer as described by Bramall *et al.* (2012) at approximately 2-week intervals from November 2010 to April 2012.

## 2.2. Spectral data reduction

Ultraviolet/visible/near-infrared transmission spectra were retrieved from the O/OREOS satellite as an average of 16 spectra with an integration time of 100 or 135 ms for each cell. Spectra were selected for further analysis based on signal levels, signal-to-noise ratio, and the extent of signal saturation. Saturation was a significant factor for the mid-mission data before collection parameters (*e.g.*, integration time, solar intensity triggers) were re-optimized. The highest-quality spectra were collected before February 2011 and after May 2011. The mid-mission gap in some of the reported results is explained by the lack of high-quality data collected during this period.

Absorbance was calculated with the following equation:

$$A = \log_{10} \left[ \frac{I_R + n}{I_S + n} \right] \quad (1)$$

where  $A$  is absorbance,  $I_S$  is the intensity of light after it passes through the sample cell, and  $I_R$  is the intensity of light after it passes through the corresponding microenvironment reference (no FeTPPCL film). These intensities were additively shifted by  $n=100$  intensity counts for presentation purposes to eliminate obfuscating noise due to low solar (light source) intensity at short wavelengths. Some of

TABLE 1. THE CONDITIONS IN EACH FeTPPCL CELL USED FOR BOTH THE FLIGHT EXPERIMENT AND SUPPORTING LABORATORY STUDIES

	<i>Film thickness</i>	<i>Number of samples</i>	<i>Substrate</i>	<i>Microenvironment</i>
Flight samples	16.5 nm	1	MgF <sub>2</sub> window	<i>Inert</i> : 100 kPa argon
		2	200 nm Al <sub>2</sub> O <sub>3</sub> film on MgF <sub>2</sub> window	<i>Atmosphere</i> : $p_{\text{CO}_2} = 1$ kPa $p_{\text{O}_2} = 0.001$ kPa balance argon to 100 kPa
		2	200 nm Al <sub>2</sub> O <sub>3</sub> film on MgF <sub>2</sub> window	<i>Humid</i> : 100 kPa argon 0.8–2.3% RH
		1	MgF <sub>2</sub> window	<i>Inert</i> : 100 kPa argon
Irradiated laboratory samples	16.5 nm	2	200 nm Al <sub>2</sub> O <sub>3</sub> film on MgF <sub>2</sub> window	<i>Atmosphere</i> : $p_{\text{CO}_2} = 1$ kPa $p_{\text{O}_2} = 0.001$ kPa balance argon to 100 kPa
		1	200 nm Al <sub>2</sub> O <sub>3</sub> film on MgF <sub>2</sub> window	<i>Humid</i> : 100 kPa argon 0.8–2.3% RH
Dark laboratory samples	16.5 nm	1	MgF <sub>2</sub> window	<i>Inert</i> : 100 kPa argon
		2	200 nm Al <sub>2</sub> O <sub>3</sub> film on MgF <sub>2</sub> window	<i>Atmosphere</i> : $p_{\text{CO}_2} = 1$ kPa $p_{\text{O}_2} = 0.001$ kPa balance argon to 100 kPa
		1	200 nm Al <sub>2</sub> O <sub>3</sub> film on MgF <sub>2</sub> window	<i>Humid</i> : 100 kPa argon 0.8–2.3% RH

our figures reflect this additive scale factor, but band integrations were done without the use of this addition. Before calculating absorbance, to correct for variations in spectral intensity from solar intensity changes due to satellite orientation,  $I_S$  was multiplicatively scaled to  $I_R$  at 330 nm, where no absorbance features were expected or detected for FeTPPCL.

### 2.3. Laboratory dark controls and irradiation experiments

Laboratory studies consisted of two segments: FeTPPCL samples that were prepared concurrently with the flight samples and kept under dark conditions, and FeTPPCL samples that were also prepared at the same time as the others and irradiated by simulated solar emission in the laboratory. The samples maintained under dark conditions were stored in an argon-purged glove box at ambient temperatures (20–25°C) and measured with UV/vis/NIR spectroscopy at approximately 30-day intervals and with mid-IR spectroscopy at six time points during the ~6-month monitoring period.

During the laboratory irradiation experiment, FeTPPCL sample cells and reference cells were photolyzed with a dual-source solar simulator. A 300 W xenon arc lamp (Newport Corporation, part no. 66485) was used to approximate the solar flux across the UV and visible wavelengths from 200 to 1000 nm at AM0 (air mass zero, *i.e.*, as in outer space at Earth's distance from the Sun). A H<sub>2</sub>/He discharge lamp was used to produce Lyman- $\alpha$  (~122 nm) radiation. H<sub>2</sub>:He partial pressure ratio was ~0.6:100; dilute mixtures result in more monochromatic Lyman- $\alpha$  output. The strength of the Lyman- $\alpha$  emission in the laboratory was measured with a UV-enhanced photodiode (method detailed in Cook *et al.*, 2014), and lamp power was adjusted until the line matched the known strength of Lyman- $\alpha$  at LEO (Vidal-Madjar, 1975). The integrated irradiance of the xenon lamp from 200–1000 nm matched that of the solar irradiance spectrum within 2%. The Lyman- $\alpha$  photon flux from the H<sub>2</sub>/He lamp was  $3.4 \times 10^{11}$  photons s<sup>-1</sup> cm<sup>-2</sup>, which is within 8% of the solar Lyman- $\alpha$  flux. The Xe and H<sub>2</sub>/He lamp beams were aligned to intersect at the target samples, covering ~1/3 of the positions in the sample carousel at a given moment. The sample carousel was rotationally stepped to bring samples in and out of the irradiation beams, exposing a given sample set to radiation for 20 s then rotating it out of the beams for 40 s before repeating the cycle. This temporal cycle was chosen to approximate the rotation rate of the O/OREOS spacecraft, which averaged about 1 rpm throughout the mission (Bramall *et al.*, 2012; Mattioda *et al.*, 2012). Temperatures inside irradiated cells were measured by using spare samples before the full solar simulation experiment was started; internal cell temperatures never exceeded 43°C and probably averaged ~35°C. A comprehensive description of the laboratory experiment, hardware, and calibration is reported in Cook *et al.* (2014).

Irradiated samples were measured at approximately 14-day intervals with a UV/vis/NIR spectrometer and with a mid-IR spectrometer at six time points throughout the experiment. Ultraviolet/visible/near-infrared spectra were recorded with an Ocean Optics HR4000CG-UV-NIR spectrometer for which a spectroscopic, fiber-coupled deuterium/halogen lamp

(DH-2000, Ocean Optics, Inc.) was used as the light source. Absorbance was calculated by using the same method described above, in Eq. 1, except that the additive scale factor  $n$  was not necessary for presentation in Fig. 3, since the laboratory spectrometer and light source provided adequate signal at short wavelengths.

A Digilab Fourier transform infrared (FTIR) spectrometer was used for all laboratory IR measurements, and band integrations were completed with Digilab Resolutions Pro software. A total of 256 scans at a resolution of 1 cm<sup>-1</sup> were averaged for the reported spectra. The resulting spectra were filtered and baseline-corrected for presentation purposes. Band area integrations were conducted on identically filtered data to remove excessive fringing due to internal reflections within the sample cell window.

Following the completion of the solar simulation and dark control experiments, sample cells were transferred to the synchrotron facility at ISA, Centre for Storage Ring Facilities, Aarhus University, Denmark (Miles *et al.*, 2007, 2008). Although the beamline at ISA is optimized for circular dichroism (CD) measurements, it can also provide normal absorption measurements. The CD1 beamline provided the capability to measure the absorbance spectra of our samples in the VUV wavelength region, from 115 to 350 nm, at a spectral resolution of 1 nm. The measurement chamber was nitrogen-purged, and the synchrotron beam entered the chamber through a CaF<sub>2</sub> window.

## 3. Results

### 3.1. Background: iron(III) tetraphenylporphyrin chloride structure and spectroscopic features

The basic structure of FeTPPCL is shown in Fig. 2. Many porphyrins are primarily planar in nature, but the metal ligand in metalloporphyrins protrudes out of the plane of the macrocycle (Lü *et al.*, 2006; El-Nahass *et al.*, 2010). The Fe, Cl, and each of the coordinating N atoms form an angle of 103.95°, raising Fe out of the macrocycle plane by almost 14° (Lü *et al.*, 2006). The crowding of the phenyl groups on the periphery of FeTPPCL is also thought to result in deformation of the macrocycle (Haddad *et al.*, 2003). Computational analysis of X-ray crystallography data by El-Nahass *et al.* (2010) determined that FeTPPCL molecules in polycrystalline powder have a tetragonal structure with lattice constants of  $a = 13.53$  Å and  $c = 9.82$  Å. The space group is I4/m,  $Z = 2$ ; that is, there are two FeTPPCL molecules per unit cell. Although thermally deposited thin films were found to be amorphous, El-Nahass *et al.* (2010) verified that the integrity of individual molecular structures is maintained at typical deposition temperatures.

Ultraviolet/visible spectra of FeTPPCL and H<sub>2</sub>TPP (tetraphenylporphyrin) have been reported by El-Nahass *et al.* (2005, 2010). In general, UV/vis spectra of porphyrins are described by the Gouterman four-orbital model, wherein absorption bands result from transitions between two HOMOs and two LUMOs (highest occupied molecular orbital and lowest unoccupied molecular orbital, respectively). A high-energy <sup>1</sup>E<sub>u</sub> state with high oscillator strength produces a strong Soret band (called the “B-band”) in the 300–480 nm region. In the case of FeTPPCL, the Soret band has a split peak, referred to as “hyper absorption” by Weinkauff *et al.* (2003); see Fig. 3. This split peak is inconsistently

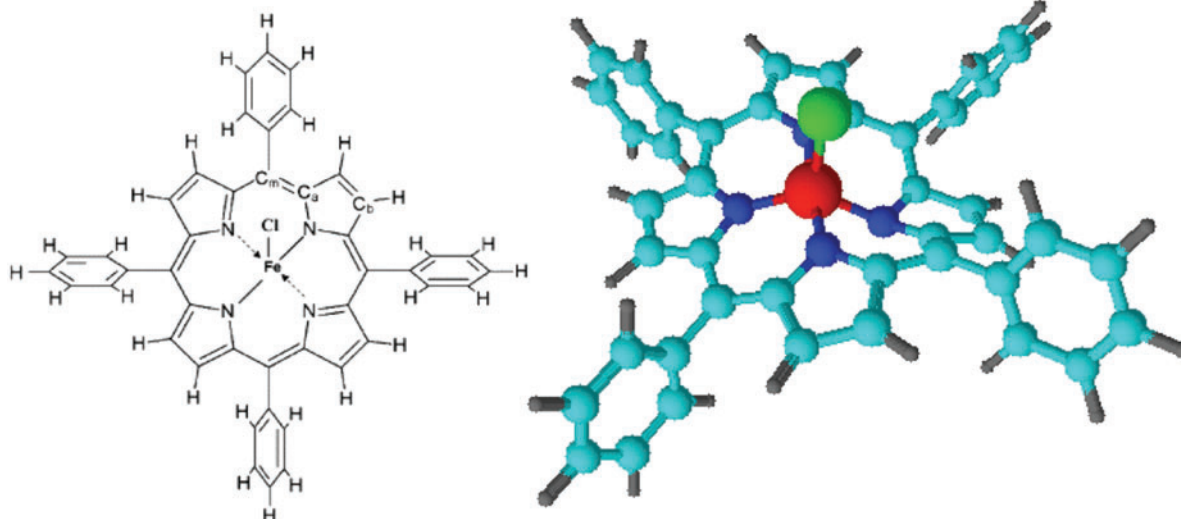


**FIG. 2.** Molecular structure of FeTPPCL. Note that the phenyl groups and metal ligand are out of the porphyrin macrocycle plane and that the typically 6-coordinate Fe(III) has only 5 ligands. Color images available online at [www.liebertonline.com/ast](http://www.liebertonline.com/ast)

identified across the literature. Weinkauff *et al.* (2003) attributed the splitting to charge transfer interactions with substituents (*e.g.*, between the porphyrin ring and the phenyl groups). According to Weinkauff *et al.* (2003) and El-Nahass *et al.* (2005), the split peaks exist in the absence of metal atoms. Therefore, as the Weinkauff study argues, intraporphyrin charge transfer is a likely explanation for double peaks, as opposed to metal-ligand or ligand-metal charge transfer, or metal-centered transfer [nominally Fe(II)  $\rightarrow$  Fe(III)]. Alternatively, Huang *et al.* (2000) attributed

the split band to opposing polarizations in the plane of the porphyrin macrocycle. These two polarizations, termed  $B_x$  and  $B_y$ , shown in Fig. 3, are degenerate and typically have almost identical intensities. The exact position and spacing of the polarization-induced split depends on the distances and angles between neighboring porphyrin molecules, any metal or other substituents, as well as the thickness of the observed film. Indeed, the  $B_x$  and  $B_y$  bands can be so closely spaced that they appear to merge into a single band in certain situations. For the sake of clarity when referring to the separate peaks in the Soret band, we adopt the  $B_x$ ,  $B_y$  terminology. Discussion of the actual peak assignments is in Section 4.

A lower-energy  $^1E_u$  state with lower oscillator strength produces a weak  $Q$  band in the region from 480 to 800 nm. Due to vibronic coupling, this band is often split into several absorptions (Nozawa *et al.*, 1980). A very weak  $N$  band is present at about 350 nm and attributed to a  $\pi$ - $d$  transition (El-Nahass *et al.*, 2010).

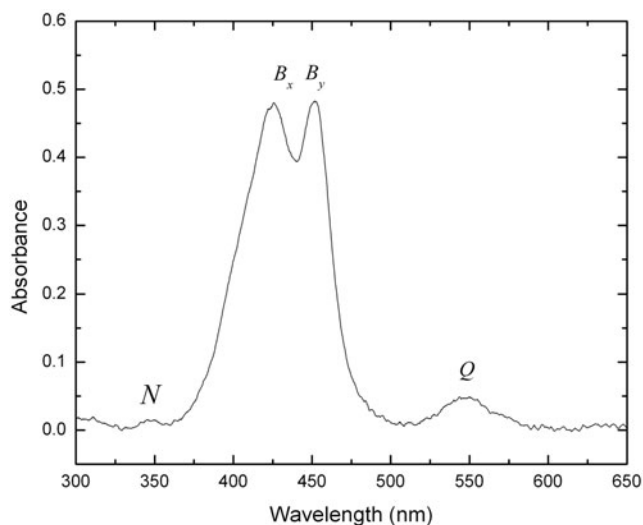


**FIG. 3.** A typical UV/vis spectrum from SEVO samples of FeTPPCL, with the molecule's apparent electronic transitions in the thin-film state. The split Soret band ( $B_x$ ,  $B_y$ ), due to the  $^1E_u$  state, is shown at  $\sim 430$  nm. The nature of the splitting depends on the thickness of the film observed as well as the porphyrin's surrounding environment. In subsequent figures, the positions of  $B_x$  and  $B_y$  are marked by vertical lines. Accompanying weak  $Q$  and  $N$  bands are visible at 550 and 350 nm, respectively. See Section 3.1 for details.

### 3.2. UV/vis spectra of flight samples

The preflight and sequential in-flight UV/vis spectra of three FeTPPCL sample cells are shown in the left-hand column of Fig. 4 (a–c). As indicated in Table 1, there were two *Atmosphere* cells and two *Humid* cells in the flight experiment, but only one of each type is shown in Fig. 4. The spectral behavior was largely consistent within cell types (*i.e.*, spectra from one *Atmosphere* cell looked like those of the other). The prominent bands with peaks at 426 and 450 nm are attributed to the  $B_x$  and  $B_y$  polarizations of the Soret band. For the *Humid* cells, these bands are merged as a broad, “single” “ $B$ ” peak centered at  $\sim 427$  nm. Another broad, but very weak, band at 550 nm is most obvious in the *Atmosphere* cell at 110 h of irradiation (Fig. 4b) but is present in varying strengths in most of the spectra. This 550 nm feature is believed to be the strongest of the  $Q$  bands, which extend with waning strength toward longer wavelengths. All the FeTPPCL flight spectra show a decrease

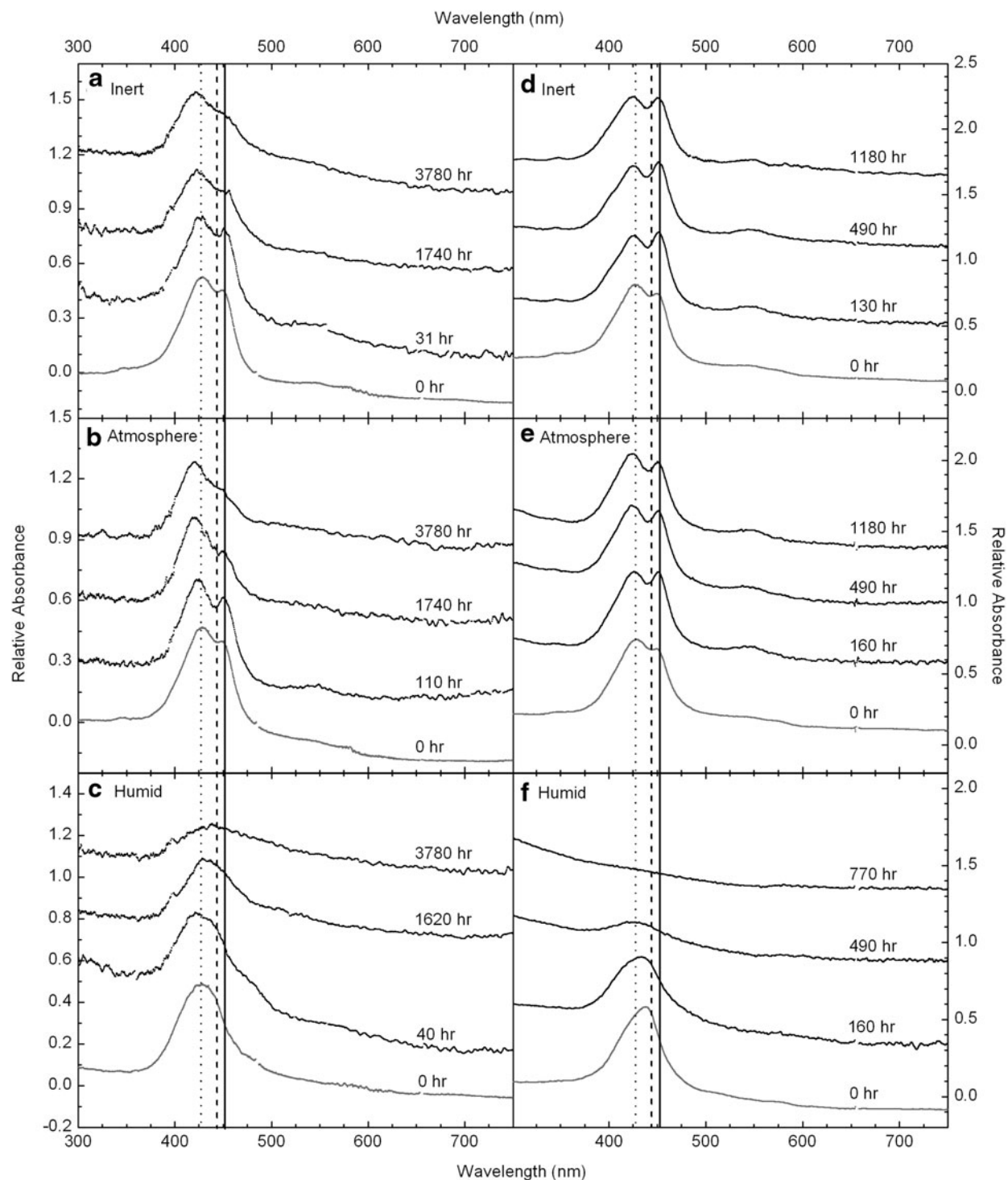


**FIG. 4.** (a–c) Ultraviolet/visible spectra of samples exposed to radiation in LEO aboard SEVO, obtained *in situ* by using the Sun as the spectroscopy light source. The bottom traces in each panel were taken before flight with a laboratory spectrometer and light source. Duplicate *Humid* and *Atmosphere* sample cells underwent similar spectral changes to those shown here. Indicated exposure times are actual time of Sun exposure, corrected for the rotation of the satellite in and out of sunlight and for periods of solar eclipse. (d–f) Ultraviolet/visible spectra of samples in the laboratory irradiation experiment. The bottom traces in each panel were taken before irradiation. Laboratory samples were exposed to a Xe full-spectrum (AM0) solar simulator combined with a H<sub>2</sub>/He discharge lamp matched to solar Lyman- $\alpha$  intensity in LEO. The duplicate *Atmosphere* cell underwent similar spectral changes to the one shown here. Indicated exposure times are actual time of solar simulator exposure, corrected for the rotation of the samples in and out of beam. The vertical dotted lines indicate the positions of the  $B_x$  Soret band component. The vertical dashed and solid lines indicate the positions of the  $B_y$  Soret component for the *Humid* and for the *Inert/Atmosphere* cells, respectively.

in absorbance over time, with the rate of change dependent on the microenvironment of the sample.

### 3.3. UV/vis spectra of irradiated laboratory samples

Ultraviolet/visible spectra from the laboratory irradiation experiments are shown in the right-hand column of Fig. 4 (d–f). Sample cells used in the laboratory experiment were exposed to simulated solar irradiation continuously for 6 months, with short breaks (<24 h) every 2 weeks for the collection of spectra. Spectra from the laboratory experiments are generally of a higher quality than the spectra obtained from the spacecraft, mainly due to the spectroscopic light source (which has better UV output than the Sun) and the ability to instantaneously optimize spectrometer parameters. The Soret band is evident in all the spectra from the laboratory experiment, and similar to the flight data, a decrease in the band is observed with increased irradiation time. Again, the rate of band loss depends on the microenvironment for each sample.

### 3.4. Integrated absorbance of the Soret region, flight and laboratory samples

To track changes in absorbance for the flight data, the entire region of the Soret band was integrated from 334 to 600 nm at numerous time points throughout the mission. Error bars for the integrated absorbance were estimated by selecting extreme (but still reasonable) continuum points on each side of the feature, resulting in the smallest and largest reasonable integrated absorbance for each spectrum, which define the margins of each error bar in Fig. 5. Larger error bars in the flight data are the result of weaker UV output from the Sun, as discussed above. The left-hand column of Fig. 5 (a–c) shows the change in integrated absorbance over time for the same cells displayed in the Fig. 4 spectra. Integrated absorbance data from each cell were fit by least-squares linear regression, weighted by error bars. Slopes and correlation coefficients ( $R$ ) for each linear fit are included in Fig. 5.

Integrations were performed for all the sample cells, including duplicates, but only one plot for each cell type is shown in Fig. 5. Linear fits to the data points have slopes in Integrated Absorbance Units (IAU) per hour of solar exposure or simulated solar exposure. The two *Humid* cells displayed the fastest decrease in the intensity of the Soret-region bands (slopes =  $-0.007$ ,  $-0.004$  IAU/h). The *Inert* and two *Atmosphere* cells showed a slower decrease in intensity of the bands (slopes =  $-0.003$ ,  $-0.002$ , and  $-0.002$  IAU/h, respectively). The error on all slopes was  $\pm 0.001$  IAU/h.

Like the flight data, spectra from the laboratory irradiation experiment were integrated from 334 to 600 nm. The changes in integrated absorbance are displayed in the right-hand column of Fig. 5 (d–f). The spectroscopic changes in the laboratory irradiation data are qualitatively similar to the flight data. Again, the *Humid* cell displays a rapid loss in intensity of the Soret-region bands, with the bands being entirely lost by  $\sim 770$  h of irradiation. The *Inert* and *Atmosphere* cells also show a decrease in the integrated band areas with time of simulated solar exposure.

Data for rates of change of absorbance versus time for each laboratory sample cell were fit with a least-squares

linear regression, weighted by error bars. Slopes and correlation coefficients ( $R$ ) for each linear fit are included in Fig. 5. The slope (rate of integrated intensity decrease) in the *Humid* cell is steeper (slope =  $-0.043$  IAU/h) than those observed for the *Inert* and two *Atmosphere* cells (slopes =  $-0.009$ ,  $-0.004$ ,  $-0.004$  IAU/h, respectively). The error on all slopes was  $\pm 0.001$  IAU/h.

### 3.5. Gaussian fitting of Soret region

Since the laboratory irradiation experiments yielded spectra with very good signal-to-noise ratios, they were found suitable for multiband curve fits, assuming Gaussian line shapes. Curve fitting was helpful to identify, analyze, and compare individual spectral components and their changes over time. Figure 6 shows four examples of the fitting. The Soret band (or bands) at 430–460 nm, the neighboring  $Q$  band at 546 nm, and the  $N$  band at 350 nm were fit with a combination of six Gaussian components. The Soret band is best fit with the largest contributions from two Gaussians,  $B_x$  and  $B_y$ , as discussed in Section 2.3. The positions of the  $B_x$  and  $B_y$  bands vary depending on the cell microenvironment. *Inert* and *Atmosphere* cells have very similar spectral shape and evolution, so we consider them together:  $B_x$  and  $B_y$  are at 428 and 452 nm for these cells, sufficiently separated to produce two distinct peaks in the Soret region. The Soret band in the *Humid* cell also has  $B_x$  and  $B_y$  components, but their respective positions at 428 and 443 nm result in an apparent (asymmetric) single peak in the Soret region. The asymmetry of this peak, however, suggests it to be a blend of the same two primary components that are more distinct in the *Inert/Atmosphere* cells. The positions of  $B_x$  and  $B_y$  are marked with vertical lines in Figs. 4 and 6. For fitting purposes, the primary  $B_x$  and  $B_y$  bands were combined with weaker, broader Gaussians, which account for shoulders on either side of the main features. These shoulders are likely the result of the amorphous structure of our FeTPPCI thin films (without the inclusion of these features, the data cannot be well fit by using Gaussian line shapes). The  $N$  band and the  $Q$  band (when apparent) were also fit with broad, but comparatively less intense, Gaussian features.

The Gaussian fits were utilized to assess relative changes in the  $B_x$  and  $B_y$  components of the Soret band over time. We supplied our fitting routine with Gaussian parameters [band centers, full widths at half maximum (FWHMs)] for only those two bands, as a first iteration. The remaining four bands (the two shoulders and the  $Q$  and  $N$  bands) were optimized with less restriction on band centers and FWHM, only after the  $B_x$  and  $B_y$  components had already been optimized. Once a reasonable fit was determined, the integrated areas of the  $B_x$  and  $B_y$  components (red traces in Fig. 6) for each irradiation time point were tabulated. The relative contributions from  $B_x$  and  $B_y$  are presented as a percentage of the total band area in Fig. 6 (e, f).

The *Humid* cell (Fig. 6e) shows a consistent decrease in the contribution of  $B_y$  to the total absorbance. The contribution from the  $B_x$  band is more persistent, accounting for 39–52% of the total absorbance at all measured time points. This strongly suggests that the structure responsible for the  $B_y$  component is preferentially eliminated with irradiation in a humid environment. Conversely, the *Inert*

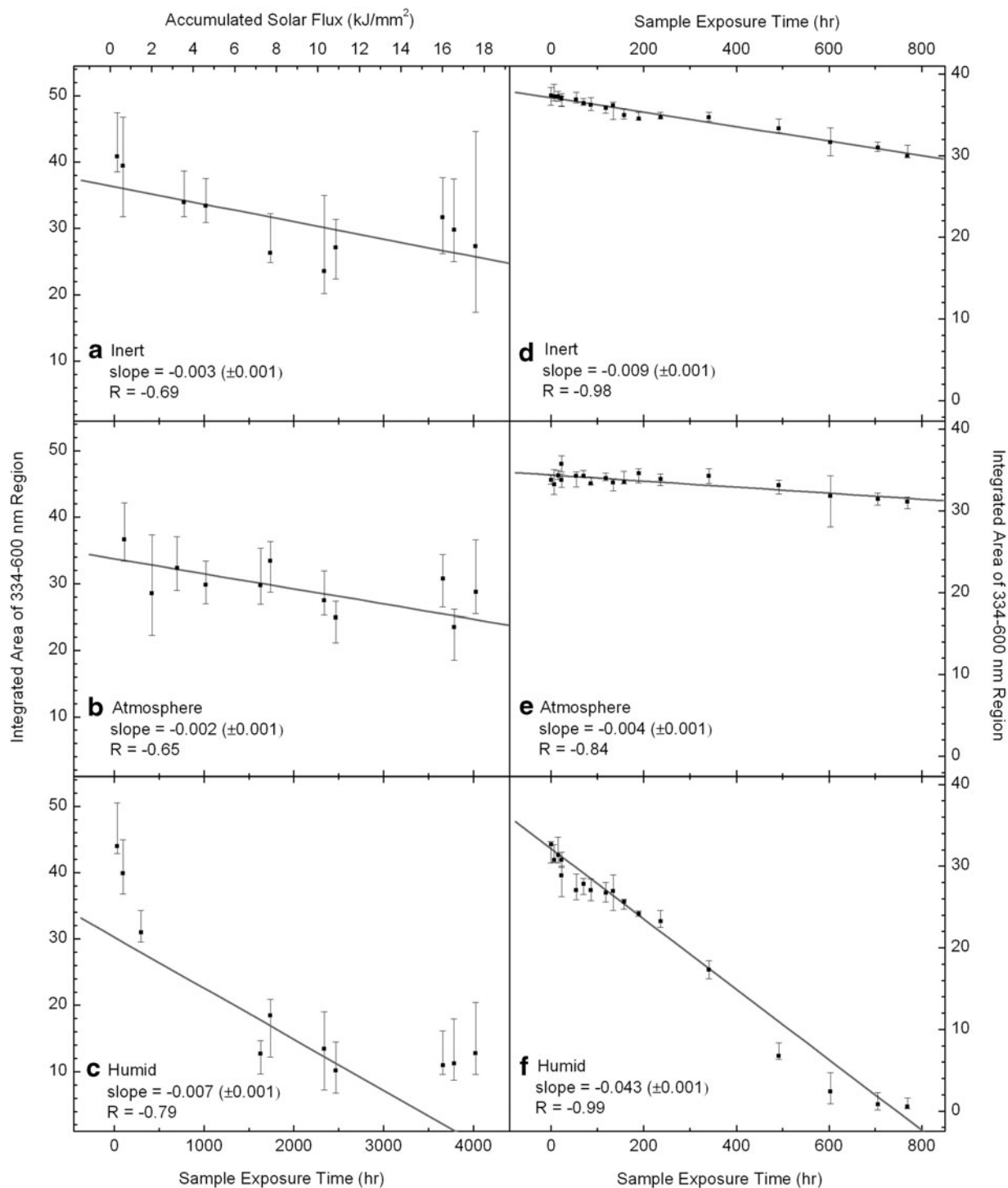


**FIG. 5.** Photo-exposure time dependence of spectral changes in the spaceflight and laboratory samples, showing correlations across the three microenvironments for integrated flight spectra (a–c) and laboratory spectra (d–f). For each spectrum, the region from 334 to 600 nm was integrated and is displayed as a function of time. Slopes (the units of which are IAU/h; see Section 3.4) and correlation coefficients ( $R$ ) for linear fits to the data are included in each panel. Plots from flight data (left-hand column) include accumulated solar flux on the upper  $x$  axis, for comparison to sample exposure time. Laboratory sample cells (right column of figure) were exposed to a Xe full-spectrum solar simulator combined with a H<sub>2</sub>/He discharge lamp matched to solar Lyman- $\alpha$  intensity in LEO. Note the comparatively rapid degradation of the integrated band area in the *Humid* cells, as compared to the *Atmosphere* and *Inert* cells.

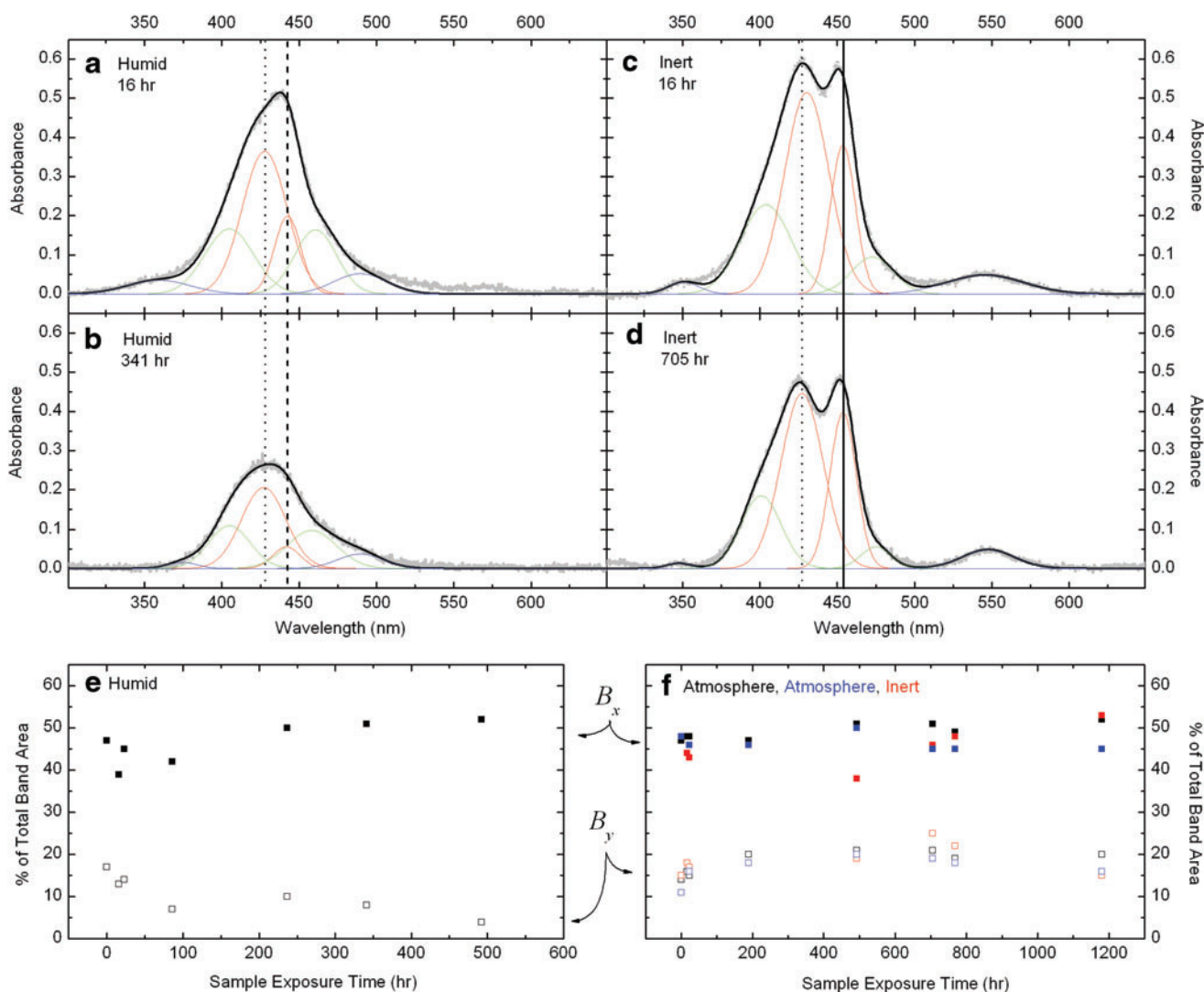


**FIG. 6.** Examples of Gaussian curve-fitting of the spectral bands. Spectra from the *Humid* cell at two time points during the laboratory irradiation experiment are presented in panels (a) and (b) as gray points; spectra from the *Inert* cell in the laboratory irradiation experiment are shown in panels (c) and (d) as gray points. Gaussian fits of spectral components are shown in red ( $B_x$  and  $B_y$ ), green (shoulders due to amorphous structure), and blue ( $N$  and  $Q$  bands). The bold black line represents the sum of the six components. As in Fig. 4, the vertical dotted lines indicate the positions of the  $B_x$  Soret band component, and the vertical dashed and solid lines indicate the positions of the  $B_y$  Soret component for the *Humid* and *Inert* cells, respectively. Note that the closer spacing of  $B_x$  and  $B_y$  (red components) in the *Humid* cell results in an apparent single peak, while the wider spacing of  $B_x$  and  $B_y$  in the *Inert* cell produces distinct double peaks. The percent contribution of the  $B_x$  and  $B_y$  components to the total absorbance is shown in panel (e) for the *Humid* cell and panel (f) for the *Inert* and two *Atmosphere* cells. For panels (e) and (f), filled squares are the band areas for the  $B_x$  component; open squares are the band areas for the  $B_y$  component. Color images available online at [www.liebertonline.com/ast](http://www.liebertonline.com/ast)

and *Atmosphere* cells display a stable (or possibly slightly increasing) contribution from the  $B_y$  band to the total Soret area and a stable (within the scatter) contribution from the  $B_x$  band.

### 3.6. UV/vis spectra of dark control samples

Four additional FeTPPCI sample cells (see Table 1) were kept under dark laboratory conditions (in an argon-purged glove box) to monitor as controls. They were measured monthly via UV/vis spectroscopy and with IR spectroscopy at two time points separated by 6 months. There were no significant changes in the UV/vis or mid-IR spectra over the monitoring period.

### 3.7. IR spectra of irradiated laboratory samples

The wavelength ranges for IR transmission through the  $\text{MgF}_2$  and sapphire ( $\text{Al}_2\text{O}_3$ ) windows employed in the SEVO cell construction limited the observable IR frequencies to those greater than  $\sim 1700\text{ cm}^{-1}$ . While there have been numerous investigations of the IR properties of tetraphenylporphyrin ( $\text{H}_2\text{TPP}$ ) and FeTPPCI (e.g., El-Nahass *et al.*, 2005; 2010), most are limited to frequencies less than  $1700\text{ cm}^{-1}$ . There appears to be a discrepancy in the literature for some of the vibrational motions above  $1700\text{ cm}^{-1}$ . In particular, the assignment of the aromatic C–H stretching modes attributed to the phenyl and the pyrrole groups are ambiguous (e.g., El-Nahass *et al.*, 2005).

To resolve this ambiguity, we conducted our own computational Density Functional Theory (DFT, see Ricca *et al.*, 2012) study to distinguish the C–H aromatic stretches of the pyrrole group in the porphyrin ring from those of the aromatic phenyl groups attached at the periphery of the ring. Our calculations showed the aromatic phenyl group C–H stretching motions to be distinct from those of the pyrrole aromatic C–H stretching, the former occurring at significantly lower frequencies than the latter. Thus, we assign the bands at  $3024$  and  $3054\text{ cm}^{-1}$  to the aromatic phenyl C–H stretch, in agreement with Saini *et al.* (2004). Figure 7 shows the positions of these bands in our thin-film samples.

The laboratory FTIR measurements shown in Fig. 7 indicate only slight changes with time in the band areas for these phenyl modes for the “dry” cells (only *Inert* cells are shown, but *Atmosphere* cells showed similar stability). However, with irradiation, the  $3024\text{ cm}^{-1}$  band undergoes a  $2\text{--}5\text{ cm}^{-1}$  redshift for the *Inert* and *Atmosphere* cells. In comparison, the phenyl aromatic stretching modes in the *Humid* cell decrease rapidly upon exposure to the solar simulator, disappearing completely from the spectrum after  $\sim 1000\text{ h}$  of irradiation; the band positions for the *Humid* cells do not appear to change with time.

Further comparison of the FTIR spectra for the three microenvironments reveals another pattern of spectral evolution. A new broad band (FWHM  $\sim 27\text{ cm}^{-1}$ ) centered at  $1961\text{ cm}^{-1}$  appears and grows with irradiation time in the *Inert* and *Atmosphere* cells. This new band is absent in the irradiated *Humid* sample cell as well as in the dark control samples. The behavior of this band and correlation plots are presented in Fig. 8 and discussed in Section 4.

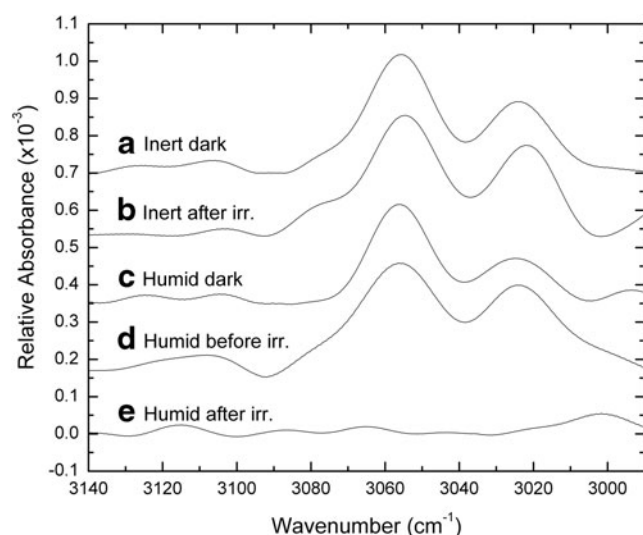


**FIG. 7.** Infrared data showing the region of aromatic phenyl C–H stretching modes in the FeTPPCL sample spectra. *Inert* and *Humid* cells are shown from the set of dark controls and the set of irradiated cells. Note that in the irradiated *Humid* cell, the aromatic phenyl bands at  $3024$  and  $3054\text{ cm}^{-1}$  have been lost by the end of radiation exposure, while the correspondingly irradiated *Inert* cell shows the phenyl bands remain intact. See Section 3.7 for details.

### 3.8. Nitrogen species in dark and irradiated laboratory samples

Vacuum ultraviolet spectra of SEVO sample cells and a SEVO window were measured at the Synchrotron Radiation Facility ASTRID at Aarhus University. Figure 9a shows the absorbance spectrum of a  $\text{MgF}_2$  window and of four complete sample cells, which are sealed with sapphire ( $\text{Al}_2\text{O}_3$ ) windows, as shown in Fig. 1b. As expected, the  $\text{MgF}_2$  window alone [*i.e.*, with no sample cell or sapphire window, trace (i)] has relatively low absorbance in the VUV/UV/vis. Likewise, the *Inert* reference cell in trace (ii) has a flat absorbance spectrum; however, the sapphire windows on these fully assembled sample cells do not transmit below  $140\text{ nm}$ . The *Atmosphere* and *Humid* reference cells [traces (iii)–(v)] present a strong, broad absorption in the VUV as a result of the additionally deposited  $\text{Al}_2\text{O}_3$  substrate layers for those cells. The VUV spectra reveal the presence of nitric oxide (NO) in the *Humid* sample cells, particularly in the dark control reference cell shown in trace (iv). The NO features marked by asterisks in Fig. 9a are also present in many of the *Humid* sample cells that were exposed to irradiation, but the strength of the bands is greatly diminished in those cells, as can be noted in trace (v) of Fig. 9a. Integration of the bands in the dark control cell indicated a NO concentration between  $300$  and  $800\text{ ppm}$ ; the concentration of NO in the irradiated *Humid* cell had an upper limit of  $180\text{ ppm}$ . NO was only detected in *Humid* cells; NO was not detected in the *Inert* or *Atmosphere* cells (see Table 1 for description of sample cell microenvironments).

*Humid* sample cells were designed to maintain a narrow range of relative humidity ( $0.8\text{--}2.3\%$  RH) inside the cell with a salt pair buffer immobilized on a stainless steel mesh at the cell’s perimeter (Bramall *et al.*, 2012). Equilibrium of  $\text{H}_2\text{O}$  between the gas phase and the salt pair depended on the temperature inside the cell. The salt pair, consisting of  $\text{Mg}(\text{NO}_3)_2$  dihydrate and  $\text{Mg}(\text{NO}_3)_2$  hexahydrate, is the only source of nitrogen in these cells (the VUV-measured cells contained no FeTPPCL). We therefore conclude that the detected NO was derived from the hydrated salt pair; NO may have originated from outgassing of impurities in the salts or from oxidation reactions involving the  $\text{H}_2\text{O}$  vapor, stainless steel mesh, and nitrate salt pair. McNesby and Fifer (1991) measured photodestruction of NO gas under  $L\alpha$  irradiation and subsequent production of  $\text{N}_2\text{O}$  and  $\text{NO}_2$ . Indeed, the loss of NO in the VUV spectra of *Humid* cells [Fig. 9a, traces (iv) and (v)] is consistent with photodestruction of this species.

Infrared spectroscopic measurements of the laboratory-irradiated *Humid* cell are shown in Fig. 9b. These IR spectra also confirm the loss of NO. Weak gas-phase P- and R-branch NO bands centered at  $1875\text{ cm}^{-1}$  are present in the *Humid* cell, at the beginning of the irradiation experiment (at 23 and 240 h). These NO bands disappear with continued irradiation. In addition, the IR spectra indicate the growth with irradiation time of P- and R-branch  $\text{N}_2\text{O}$  bands centered at  $2224\text{ cm}^{-1}$ .  $\text{NO}_2$  bands, if they exist, would be strongest around  $1600\text{ cm}^{-1}$ . Since this frequency is outside the observable range for our SEVO cells, we were not able to confirm or eliminate the possibility of the presence of this molecule in our sample cells.

## 4. Discussion

Ultraviolet/visible spectral changes were measured for FeTPPCL in each of the three microenvironments, in both the

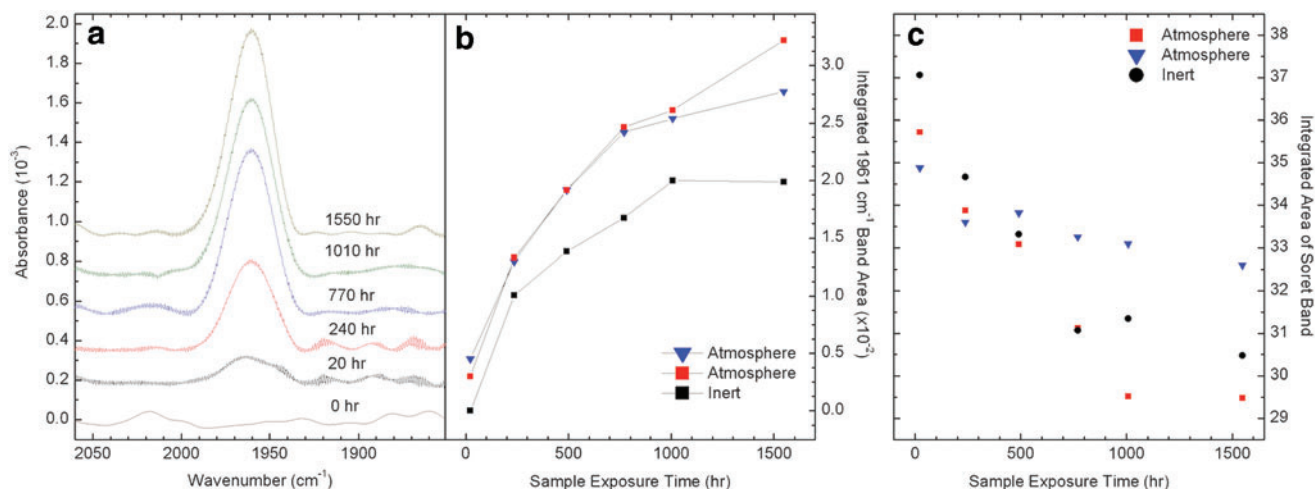


**FIG. 8.** Infrared data, integrated bands, and correlations. (a) Growth of a new band at  $1961\text{ cm}^{-1}$  over the duration of laboratory irradiation of FeTPPCL in the *Atmosphere* microenvironment. Irradiation time points are listed in hours. (b) Integrated area of the  $1961\text{ cm}^{-1}$  band over time of exposure to irradiation for the three cells (two *Atmosphere* and one *Inert*) in which the band was detected. (c) Correlation plot, comparing the total integrated absorbance of the Soret band to the integrated area of the  $1961\text{ cm}^{-1}$  band for the same cells and irradiation time points. Note the increase in the  $1961\text{ cm}^{-1}$  band and the decrease in the Soret band. Color images available online at [www.liebertonline.com/ast](http://www.liebertonline.com/ast)

flight experiment and the laboratory experiment. The overall character and evolution of both the *Inert* and *Atmosphere* sample spectra are very similar for flight and ground samples (Figs. 4 and 5); indeed, comparison of these sample types in the flight and lab experiments shows a similar (within a factor of 2–3) rate of loss of total absorbance in both cases (Fig. 5). Both sample types also show an  $\sim 8\text{ nm}$  blue-ward shift in the position of the  $B_x$  band with continued irradiation. We con-

clude that dry headspace gas is the primary factor in their similar behavior. The presence of  $\text{CO}_2$  and  $\text{O}_2$  in the *Atmosphere* cells, as well as the wavelength-filtering substrate coatings for these cells, plays at best a minor role in the spectral evolution of *Atmosphere* relative to *Inert* samples: Figure 5 shows that disappearance rates are  $\sim 1.5\text{--}2\times$  slower for the *Atmosphere* relative to the *Inert* samples in the flight and laboratory exposure experiments.

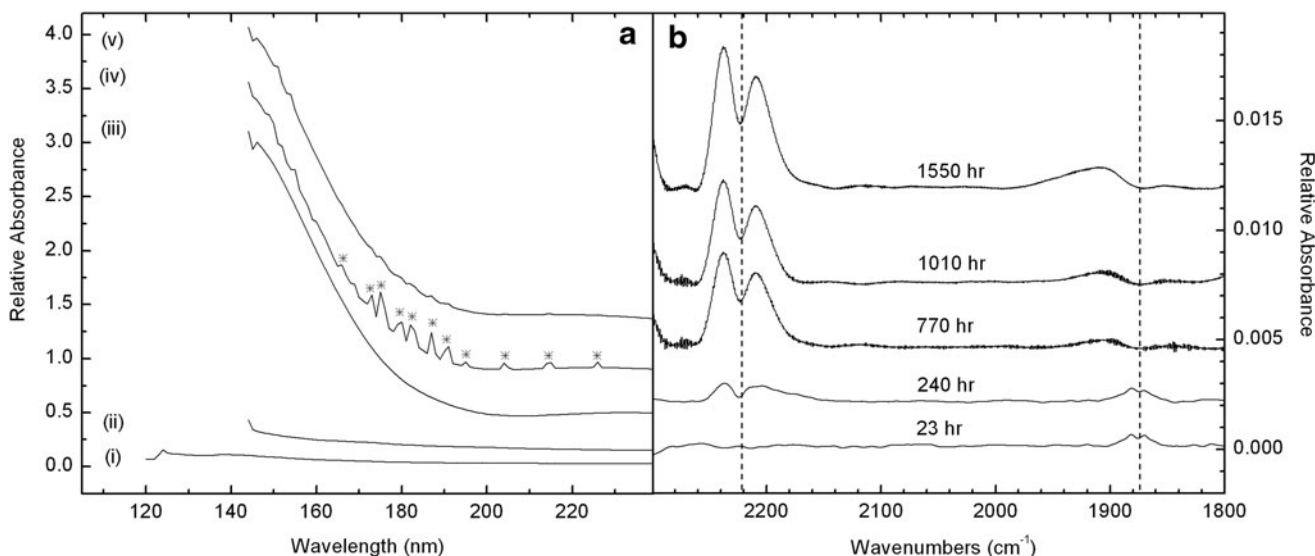


**FIG. 9.** (a) Vacuum ultraviolet spectra of SEVO sample cells at the conclusion of the laboratory irradiation experiment. Individual traces show the absorbance spectrum of (i) a  $\text{MgF}_2$  window only, from a disassembled cell, (ii) an *Inert* reference cell from the irradiation experiment, (iii) an *Atmosphere* cell from the set of dark control samples, (iv) a *Humid* cell from the set of dark control samples, and (v) a *Humid* cell from the irradiation experiment. Nitric oxide features, marked with asterisks, are present in (iv) and also (very weakly) in (v). (b) Infrared spectra of the irradiated FeTPPCL *Humid* cell, with increasing irradiation exposure time. The gas-phase P branch for  $\text{N}_2\text{O}$  is visible at  $2224\text{ cm}^{-1}$ , and the R branch for NO is visible at  $1875\text{ cm}^{-1}$ . Note the increasing strength of the  $\text{N}_2\text{O}$  band and the apparent decrease of the band associated with NO as exposure time increases. See Section 3.8 for details.

In contrast to the “dry” samples discussed above, the *Humid* samples showed more rapid degradation of the FeTPPCL with time of exposure. Photogenerated OH· was expected to play a major role in this accelerated degradation, which is consistent with its destructive capabilities. However, the presence of NO (as well as N<sub>2</sub>O) may have played a role in the degradation of the films in these cells as well. Based on humidity levels inside the cells, the concentration of H<sub>2</sub>O was ~450 ppm. As noted in the previous section, NO concentrations were between 300 and 800 ppm in non-irradiated cells and decreased to <180 ppm after 1180 h of laboratory irradiation. By contrast, H<sub>2</sub>O gas was still detectable in IR spectra of the *Humid* sample cells, even after irradiation. NO and OH· are both odd electron (radical) species, and the dark results show that light is required for degradation in any case. However, the persistence of H<sub>2</sub>O gas and the decrease of NO in the *Humid* cells support our hypothesis that photogenerated OH· played an important role in the degradation of the porphyrin.

Wayland and Olson (1974) found that FeTPPCL exposed to higher partial pressures of NO (~1000 times higher than the NO pressure in our sample cells) readily produced FeTPP(NO)Cl and, in the presence of a weak reducing agent, FeTPP(NO). Our IR spectra show no clear evidence of the band detected by the authors at 1870 cm<sup>-1</sup>, which is related to a linear Fe(II)NO<sup>+</sup> unit. In our UV/vis spectra (Fig. 4), there is some evidence of a new band at 400 nm, but this band is present in the *Inert* cell type as well; since the *Inert* samples do not contain any NO, the 400 nm band cannot be attributed to the FeTPP(NO) band detected at that wavelength by Wayland and Olson (1974). The more likely explanation for the 400 nm feature is a variation in the solar spectrum over time, in which particular absorption lines (Ca<sup>+</sup> has two closely spaced lines at 398 and 396 nm) increase or decrease due to solar activity.

While, on the whole, all *Humid* cells showed a more rapid loss in FeTPPCL than the dry *Inert* and *Atmosphere* samples, the laboratory experiment showed much more rapid degradation with time of exposure than the corresponding spaceflight samples. The rate of decrease of integrated absorbance for the laboratory-irradiated samples is a factor of ~6 times higher than the rate observed in the flight experiment (Fig. 5). The most plausible explanation for this difference is the effect that temporal thermal and illumination exposure variations in the spaceflight sample cells have on the environment inside the *Humid* cells. Humidity is maintained within a certain range (0.8–2.3% RH) by a hydrated salt-pair buffer, with the humidity within this range being determined by the sample cell temperature (higher temperature results in higher water vapor pressure). In orbit, sample cell temperatures depend on the satellite's orientation relative to the Sun, as well as its position in and out of Earth's shadow. On average, during each 98 min orbit, the satellite spent approximately 1/3 of the time in Earth's shadow, although this fraction varied from near zero to over 50% at different phases of the orbit over the course of months. For the spaceflight experiment, the concentration of photogenerated OH· in the *Humid* cells would drop quickly during the shadowed portion of each rotation of the satellite about its axis; a similar effect occurs during the 40 s time periods (out of each minute) during which the laboratory samples are in the dark. In the space experiment, the con-

centration of photogenerated OH· also would fall to zero during the many-minutes-long periods of eclipse during each orbit of Earth. In the laboratory exposure, there was no analogous “long dark period” except on those occasions when samples were removed for spectroscopic measurements. Further, the average temperature of samples in the laboratory experiment (~30°C, based on a range of 20–43°C) was higher most of the time than for the flight samples exposed to varying temperatures, resulting in higher relative humidity within the laboratory cells and, presumably, higher concentrations of photogenerated OH· in contact with those samples. Organics are expected to degrade more rapidly in the presence of highly reactive OH·; in the laboratory *Humid* sample relative to the flight sample, faster destruction of the FeTPPCL was unequivocally measured.

Other studies have addressed the fidelity of laboratory-simulated solar irradiation. Guan *et al.* (2010) conducted experiments to compare the effects of simulated radiation to that experienced in LEO and contended that many different variables can cause differences in observed processing of organics in space and in a laboratory simulation. These factors include pressure, gas mixture ratios, and power used in H<sub>2</sub>(/He) lamps to produce Lyman- $\alpha$  irradiation (all of which affect the monochromaticity and spectral distribution of the lamp output), decrease in transmission of MgF<sub>2</sub> windows due to extended irradiation time (color centers), as well as temperature fluctuations.

As noted in Section 3.5, the *Humid* sample displayed a preferential loss of the B<sub>y</sub> (443 nm) polarization of the Soret band compared to the B<sub>x</sub> (428 nm) polarization. Eventually, the entire Soret band was lost, but B<sub>y</sub> disappeared first according to our Gaussian fits to laboratory data. Differences in the two polarization components have been ascribed to such factors as distances and angles between neighboring porphyrins, differences in metal or other substituents, as well as the thickness of the film (Huang *et al.*, 2000). For the thin films (~17 nm) studied here, the presence or absence of water presents a likely cause of polarization component differences; the Fe in FeTPPCL is formally coordinatively unsaturated, being ligated by four nitrogen atoms in the plane of the porphyrin and one axial Cl<sup>-</sup>. In the solid state, Fe's 6<sup>th</sup> coordination is likely satisfied by weak bonding to one of the nitrogen electron lone pairs of a neighboring FeTPPCL, which is consistent with the Z=2 variation of the crystal structure's space group (El-Nahass *et al.*, 2010). The thin-film form of this compound provides ready access for H<sub>2</sub>O to Fe's 6<sup>th</sup> coordination site for those molecules at or near the outer surface, and any grain boundaries could provide access to some fraction of the molecules within the film as well. This “free” H<sub>2</sub>O (or OH<sup>-</sup>, with the dissociated H<sup>+</sup> finding a nearby N from an adjacent porphyrin ring) would serve as a better 6<sup>th</sup> ligand for Fe than the geometrically constrained, shared N lone pairs. The addition of an axial H<sub>2</sub>O or OH<sup>-</sup> ligand could thus be the cause of different ratios of B<sub>x</sub>, B<sub>y</sub> polarization components for samples in humid versus dry environments. It could also be the reason for the differential rate of change in the two polarization states as new areas of the film are opened to water access by the photodegradation process.

The decreasing B<sub>y</sub> band was also compared with the loss of IR features in the same cell (particularly the aromatic bands at 3024 and 3054 cm<sup>-1</sup>). Unfortunately, the B<sub>y</sub> feature

was completely lost in the UV/vis spectra before more than three data points (for integrated absorbance) could be collected via mid-IR spectroscopy. With only these three available points, there does not appear to be a correlation between the loss of aromatic bands ( $3034, 3054\text{ cm}^{-1}$ ) in the IR and the loss of the  $B_y$  band in the UV/vis.

The observed UV/vis spectral changes of the thin films were further examined by IR studies. The appearance and growth of a new band around  $1961\text{ cm}^{-1}$  is intriguing, considering the limited changes observed in the phenyl aromatic C–H stretching region, which indicate that the phenyl groups are still intact in the *Inert* and *Atmosphere* cells. Furthermore, when cells were disassembled and exposed to air, this band disappeared, indicating a sensitivity to moisture or oxygen.

The growth of the  $1961\text{ cm}^{-1}$  band was compared to the loss of the Soret band in the UV/vis spectra of the *Inert* and *Atmosphere* cells. Infrared spectra were measured at six time points throughout the laboratory experiment, and unlike the *Humid* sample, the *Inert* and *Atmosphere* samples degraded slowly enough that their bands were detectable with UV/vis spectroscopy over the entire duration of the laboratory experiment. An inverse correlation between the  $1961\text{ cm}^{-1}$  band and the total absorbance of the Soret region is shown in Fig. 8c. The inverse correlation ( $R$ ) was strong for each of the sample cells (*Atmosphere*,  $R = -0.83, -0.97$ ; *Inert*,  $R = -0.94$ ), indicating that the growth of the  $1961\text{ cm}^{-1}$  band is likely to be related to the destruction of the porphyrin ring.

Given the limited IR window available for our study, unequivocal identification of the species responsible for the  $1961\text{ cm}^{-1}$  band is not possible; however, a literature search for relevant molecules exhibiting a vibrational band in that region resulted in several possibilities: benzene ( $\text{C}_6\text{H}_6$ ), an iron carbonyl complex, ethynylmethyl iron ( $\text{CH}_3\text{FeC}_2\text{H}$ ), chloropropadiene ( $\text{C}_3\text{H}_3\text{Cl}$ ), and allene ( $\text{C}_3\text{H}_4$ ). Upon irradiation, it is possible that the porphyrin ring is destroyed, leaving behind phenyl groups to form benzene, which exhibits an intense band around  $1961\text{ cm}^{-1}$ . However, benzene should also exhibit a band nearly as intense at  $1815\text{ cm}^{-1}$ ; this band is not visible in our spectra, so we eliminate this option. FeTPP carbonyl complexes could be formed from contaminant oxygen in the *Inert* cell or  $\text{CO}_2$  in the *Atmosphere* cells. These complexes tend to exhibit intense bands in the  $1950\text{--}1975\text{ cm}^{-1}$  region of the IR spectrum. Wayland *et al.* (1978) reported that when FeTPP in solution was exposed to an atmosphere of CO, they detected growth of a band at  $1973\text{ cm}^{-1}$ . They assigned the band to FeTPP(CO). The  $\text{CO}_2$  and  $\text{H}_2\text{O}$  contamination in our sample cells is estimated to be at very low part-per-million levels, so it is unlikely to be responsible for the growth of this band in our *Inert* cell, which nominally contains no source of oxygen. We therefore conclude that, barring improbable contamination levels, carbonyl complexes are an unlikely source of the  $1961\text{ cm}^{-1}$  band.

As discussed by Bartocci *et al.* (1991) and Ball *et al.* (1993, 1994), the iron atom in metalloporphyrins can act as a catalyst under UV irradiation. In the studies of Ball *et al.* (1993, 1994), allene and methylacetylene with atomic iron were irradiated in an argon matrix. In both instances, when irradiated at wavelengths between 280 and 360 nm, a series of bands grew in between  $1960$  and  $1980\text{ cm}^{-1}$ . The authors

attributed the new bands to the  $\text{C}\equiv\text{C}$  stretch of the ethynyl group ( $\text{C}_2\text{H}$ ). This species did not form when diatomic iron was used in the experiments. However, the Ball *et al.* (1993, 1994) studies indicate that the formation of this compound may require the availability of isolated Fe atoms, which are not likely to be present in our thin film samples. Chloropropadiene presents another possible candidate for the  $1961\text{ cm}^{-1}$  feature. Shimanouchi (1972) reported a band at  $1963\text{ cm}^{-1}$  ( $\text{C}\equiv\text{C}$  stretch); we hypothesize that this species could be created via UV reduction of Fe(III) to Fe(II), subsequently removing the  $\text{Cl}^-$  ion (and freeing one electron). The  $\text{Cl}^-$  may react with the porphyrin ring to make  $\text{C}_3\text{H}_3\text{Cl}$ . This compound would not be found in the *Humid* samples (indeed, there is no  $1961\text{ cm}^{-1}$  feature in the irradiated *Humid* cells), since  $\text{Cl}^-$  would be more likely to react with  $\text{H}_2\text{O}$  to form HCl.

Finally, allene exhibits a  $\text{C}\equiv\text{C}$  stretch around  $1957 (\pm 6)\text{ cm}^{-1}$  (Shimanouchi, 1972), as well as a  $\text{CH}_2$  symmetric stretch around  $3015\text{ cm}^{-1}$  in the gas phase. Additionally, it is possible that the redshift of the phenyl aromatic band at  $3024\text{ cm}^{-1}$  is the result of the formation of allene (where allene is replacing the contribution from phenyl groups). Considering all the factors discussed above as well as the relevant literature, we conclude that the most likely candidates for the new band at  $1961\text{ cm}^{-1}$  are chloropropadiene and allene. Additional experiments are planned to study the formation of irradiation products, particularly in the IR, without frequency-limiting windows on the cells.

Regardless of the molecular species responsible for the feature around  $1961\text{ cm}^{-1}$ , it is clear that the chemical evolution processes that occurred in the *Humid* cell are distinct from those of either the *Inert* or *Atmosphere* cells. In the *Humid* cell, it appears that the phenyl aromatic rings responsible for the aromatic bands at  $3024$  and  $3055\text{ cm}^{-1}$  were completely destroyed. In contrast, the aromatic phenyl bands persist in the *Atmosphere* and *Inert* cells, albeit with measurable redshifts. In addition, the chemical processes that occurred in the *Atmosphere* and *Inert* cells appear to be similar, implying that the  $\text{CO}_2$  and  $\text{O}_2$  in the *Atmosphere* cells did not play a measurable role in the modification of FeTPPCI.

## 5. Summary and Conclusions

The SEVO experiment on board O/OREOS has successfully measured and telemetered time-evolved spectra of FeTPPCI samples exposed to solar irradiation and space conditions in LEO. To aid in the interpretation of these data, a laboratory experiment was developed for exposure of nominally identical FeTPPCI samples to a high-fidelity (over the  $122\text{--}1000\text{ nm}$  range) solar simulator. All the irradiated thin-film FeTPPCI samples, in contact with astrobiologically relevant “microenvironments,” showed degradation in response to irradiation, both in space and in the lab. Dark control samples remained unchanged.

It was found that FeTPPCI, a member of the porphyrin class of organic molecules, was more readily photodegraded in our *Humid* microenvironment ( $0.8\text{--}2.3\%$  RH) than in the drier (low ppm  $\text{H}_2\text{O}$  levels) *Inert* and *Atmosphere* microenvironments (argon and  $\text{CO}_2\text{:CO:O}_2$  headspace gases, respectively). While the FeTPPCI thin-film samples degraded in all the microenvironment cells, the photodegradation rate

was more rapid in the *Humid* cell, by a factor of  $\sim 2$ – $3$  in the flight experiment and a factor of  $\sim 5$ – $10$  in the laboratory irradiation experiment, than for the corresponding “dry” samples. The observed degradation of UV/vis features in the *Humid* sample cells is attributed to an initial loss of aromatic phenyl groups, followed by destruction of the porphyrin ring itself, based on our IR studies of the samples, which indicated the loss of aromatic C–H stretching features at 3024 and 3055  $\text{cm}^{-1}$ . These findings imply that wet, NO-rich environments, in combination with UV irradiation, encourage more efficient degradation of porphyrin-class organics. This might indicate that dry planetary surfaces with an absence of nitric oxide and/or with atmospheric screening of UV radiation could allow porphyrin structures to be preserved over longer timescales than otherwise similar wet environments.

These findings complement the Mattioda *et al.* (2012) study, which reported results for a large polycyclic aromatic hydrocarbon (PAH) and a quinone. The PAH was also found to be measurably less stable under irradiation in a humid environment. The chemical pathway for degradation of the PAH likely involves OH $\cdot$  radicals produced from H $_2$ O vapor interacting with and destroying these molecules. The detection of NO in the *Humid* sample cells also introduces the possibility that the PAH destruction was influenced by this species. However, as is the case with FeTPPCL, the PAHs were only degraded in the UV-exposed samples. The presence of nitric oxide appears to have had no destructive effect on the PAH samples in the absence of irradiation.

Observed degradation in the *Inert* and *Atmosphere* cells is correlated with the growth of a new band at 1961  $\text{cm}^{-1}$ . Pending future study, we hypothesize that this band is associated with a photodegradation product, most likely allene or chloropropadiene. We further conclude that the growth of this band is the result of destruction of the porphyrin ring (*i.e.*, probably not related to the attached phenyl groups on FeTPPCL), based on correlations with band loss in the UV/vis.

While the laboratory solar simulator results reported in this paper are clearly helpful when interpreting our analogous spaceflight results, the discrepancies noted in this paper also make it clear that greater fidelity in matching temporal variations in temperature and photon exposure will be required if laboratory kinetic data are to match or even predict those of spaceflight samples. Due to the demonstrable differences that result from imperfect simulations, it remains difficult to compare results between different laboratories and different experiments.

The results of the reported experiments also show how different microenvironments (*e.g.*, the presence of a few % RH or the presence of oxides of nitrogen) strongly influence the complex pattern of photodegradation of a metalloporphyrin. Given the importance of porphyrins as potential biomarkers, it is essential to understand their behavior under relevant astrobiological conditions. In the case of FeTPPCL thin films in contact with a humid headspace gas containing NO, it appears that aromatic phenyl side-groups may be the first fragments formed upon degradation of the molecule. However, in dry environments this molecule is quite robust. This suggests that FeTPPCL is a viable biomarker in low-humidity (or totally dry) environments, and given its slow rate of degradation, it may be possible to estimate surface exposure times, if the molecule were to be detected on planetary surfaces and the environmental conditions were well known.

## Acknowledgments

The authors would like to thank the NASA Astrobiology Small Payloads program for support, Robert Walker for technical support, Emmett Quigley and Ryan Walker of the NASA Ames Airborne Instrument Development Lab for their work in producing the hardware necessary for the production of the sample cells and the glove box experiment. We thank Dr. El-Nahass at Ain Shams University for useful discussion regarding the nature of our porphyrin spectra. The authors also thank the NASA Astrobiology Institute, the NASA Postdoctoral Program (NPP) administered by Oak Ridge Associated Universities through a contract with NASA, and the Exobiology Program for additional support (proposal number 09-EXO09-1030). We also thank Cindy Taylor for assistance with deposition and characterization of the thin films, and members of the NASA Ames Small Spacecraft Payloads and Technologies Team. We are also grateful for the efforts of the highly effective student-and-staff O/OREOS mission operations team at Santa Clara University.

## Abbreviations

AM0, air mass zero; FeTPPCL, iron(III) tetraphenylporphyrin chloride; FTIR, Fourier transform infrared; FWHM, full width at half maximum; IAU, Integrated Absorbance Units; LEO, low-Earth orbit; NIR, near-infrared; O/OREOS, Organism/Organic Exposure to Orbital Stresses; PAH, polycyclic aromatic hydrocarbon; SEVO, Space Environment Viability of Organics; VUV, vacuum ultraviolet.

## References

- Ball, D.W., Pong, R.G.S., and Kafafi, Z.H. (1993) Reactions of atomic and diatomic iron with allene in solid argon. *J Am Chem Soc* 115:2864–2870.
- Ball, D.W., Pong, R.G.S., and Kafafi, Z.H. (1994) Reactions of atomic and diatomic iron with methylacetylene in solid argon. *J Phys Chem* 98:10720–10727.
- Bartocci, C., Maldotti, A., Varani, G., Battioni, P., Carassiti, V., and Mansuy, D. (1991) Photoredox and photocatalytic characteristics of various iron *meso*-tetraarylporphyrins. *Inorg Chem* 30:1255–1259.
- Bramall, N.E., Quinn, R., Mattioda, A., Bryson, K., Chittenden, J.D., Cook, A., Taylor, C., Minelli, G., Ehrenfreund, P., Ricco, A.J., Squires, D., Allamandola, L.J., and Hoffmann, S.V. (2012) The development of the Space Environment Viability of Organics (SEVO) experiment aboard the Organism/Organic Exposure to Orbital Stresses (O/OREOS) satellite. *Planet Space Sci* 60:121–130.
- Bryson, K.L., Peeters, Z., Salama, F., Foing, B., Ehrenfreund, P., Ricco, A.J., Jessberger, E., Bischoff, A., Breitfellner, M., Schmidt, W., and Robert, F. (2011) The ORGANIC experiment on EXPOSE-R on the ISS: flight sample preparation and ground control spectroscopy. *Adv Space Res* 48:1980–1996.
- Cook, A.M., Mattioda, A.L., Quinn, R.C., Ricco, A.J., Ehrenfreund, P.E., Bramall, N.E., Minelli, G., Quigley, E., Walker, R., and Walker, R. (2014) SEVO on the ground: design of a laboratory solar simulation in support of the O/OREOS mission. *Astrophys J Suppl Ser* 210:15–22.
- Dever, J.A., Miller, S.K., Sechkar, E.A., and Wittberg, T.N. (2008) Space environment exposure of polymer films on the Materials International Space Station Instrument: results from MISSE 1 and MISSE 2. *High Perform Polym* 20:371–387.

- Ehrenfreund, P., Ricco, A.J., Squires, D., Kitts, C., Agasid, E., Bramall, N., Bryson, K., Chittenden, J., Conley, C., Cook, A., Mancinelli, R., Mattioda, A., Nicholson, W., Quinn, R., Santos, O., Tahu, G., Voytek, M., Beasley, C., Bica, L., Diaz-Aguado, M., Friedericks, C., Henschke, M., Landis, D., Luzzi, E., Ly, D., Mai, N., Minelli, G., McIntyre, M., Neumann, M., Parra, M., Piccini, M., Rasay, R., Ricks, R., Schooley, A., Stackpole, E., Timucin, L., Yost, B., and Young, A. (2014) The O/OREOS mission—astrobiology in low Earth orbit. *Acta Astronaut* 93:501–508.
- El-Nahass, M.M., Zeyada, H.M., Aziz, M.S., and Makhlof, M.M. (2005) Optical absorption of tetraphenylporphyrin thin films in UV/vis-NIR region. *Spectrochim Acta A Mol Biomol Spectrosc* 61:3026–3031.
- El-Nahass, M.M., El-Deeb, A.F., Metwally, H.S., and Hassani, A.M. (2010) Structural and optical properties of iron (III) chloride tetraphenylporphyrin thin films. *European Physical Journal Applied Physics* 52:10403–10411.
- Guan, Y.Y., Fray, N., Coll, P., Macari, F., Chaput, D., Raulin, F., and Cottin, H. (2010) UVolution: compared photochemistry of prebiotic compounds in low Earth orbit and in the laboratory. *Planet Space Sci* 58:1327–1346.
- Haddad, R.E., Gazeau, S., Pecaut, J., Marchon, J.-C., Medforth, C.J., and Shelnut, J.A. (2003) Origin of the red shifts in the optical absorption bands of nonplanar tetraalkylporphyrins. *J Am Chem Soc* 125:1253–1268.
- Huang, X., Nakanishi, K., and Berova, N. (2000) Porphyrins and metalloporphyrins: versatile circular dichroic reporter groups for structural studies. *Chirality* 12:237–255.
- Johnson, F.M. (2006) Diffuse interstellar bands: a comprehensive laboratory study. *Spectrochim Acta A Mol Biomol Spectrosc* 65:1154–1179.
- Kinard, W., O'Neal, R., Wilson, B., Jones, J., Levine, A., and Calloway, R. (1994) Overview of the space environmental effects observed on the retrieved Long Duration Exposure Facility (LDEF). *Adv Space Res* 14:7–16.
- Lü, Q.-Z., Lu, Y., and Wang, J.-J. (2006) DFT study of iron tetraphenylporphyrin chloride and iron pentafluorophenylporphyrin chloride. *Chinese Journal of Chemical Physics* 19:227–232.
- Mattioda, A., Cook, A., Ehrenfreund, P., Quinn, R., Ricco, A.J., Squires, D., Bramall, N., Bryson, K., Chittenden, J., Minelli, G., Agasid, E., Allamandola, L., Beasley, C., Burton, R., Defouw, G., Diaz-Aguado, M., Fonda, M., Friedericks, C., Kitts, C., Landis, D., McIntyre, M., Neumann, M., Rasay, M., Ricks, R., Salama, F., Santos, O., Schooley, A., Yost, B., and Young, A. (2012) The O/OREOS mission: first science data from the Space Environment Viability of Organics (SEVO) payload. *Astrobiology* 12:841–853.
- McNesby, K.L. and Fifer, R.A. (1991) *Fourier Transform Infrared Spectroscopy of Nitric Oxide During Exposure to Vacuum Ultraviolet Radiation*, Ballistic Research Laboratory Technical Report BRL-TR-3212, Ballistic Research Laboratory, Aberdeen Proving Ground, MD.
- Miles, A.J., Hoffmann, S.V., Tao, Y., Janes, R.W., and Wallace, B.A. (2007) Synchrotron radiation circular dichroism (SRCD) spectroscopy: new beamlines and new applications in biology. *Spectroscopy* 21:245–255.
- Miles, A.J., Janes, R.W., Brown, A., Clarke, D.T., Sutherland, J.C., Tao, Y., Wallace, B.A., and Hoffmann, S.V. (2008) Light flux density threshold at which protein denaturation is induced by synchrotron radiation circular dichroism beamlines. *J Synchrotron Radiat* 15:420–422.
- Nicholson, W.L., Ricco, A.J., Mancinelli, R., Santos, O., Ly, D., Parra, M., Ehrenfreund, P., Squires, D., Kitts, C., Agasid, E., Beasley, C., Diaz-Aguado, D., Friedericks, C., Ghassemieh, S., Hines, J.W., Henschke, M., Luzzi, E., Mai, N., McIntyre, M., Neumann, M., Minelli, G., Piccini, M., Rasay, R., Ricks, R., Schooley, A., Timucin, L., Yost, B., and Young, A. (2011) The O/OREOS mission: first science data from the Space Environment Survivability of Living Organisms (SE-SLO) payload. *Astrobiology* 11:951–958.
- Nozawa, T., Kobayashi, N., Hatano, M., Ueda, M., and Sogami, M. (1980) Magnetic circular dichroism on oxygen complexes of hemoproteins: correlation between magnetic circular dichroism magnitude and electronic structures of oxygen complexes. *Biochim Biophys Acta* 626:282–290.
- Rabbow, E., Rettberg, P., Barczyk, S., Bohmeier, M., Parpart, A., Panitz, C., Horneck, G., von Heise-Rotenburg, R., Hoppenbrouwers, T., Willnecker, R., Baglioni, P., Demets, R., Dettmann, J., and Reitz, G. (2012) EXPOSE-E: an ESA astrobiology mission 1.5 years in space. *Astrobiology* 12:374–386.
- Ricca, A., Bauschlicher, C.W., Boersma, C., Tielens, A.G.G.M., and Allamandola, L.J. (2012) The infrared spectroscopy of compact polycyclic aromatic hydrocarbons containing up to 384 carbons. *Astrophys J* 754, doi:10.1088/0004-637X/754/1/75.
- Saini, G.S.S., Sharma, S., Kaur, S., Tripathi, S.K., and Mahajan, C.G. (2004) Infrared spectroscopic studies of free-base tetraphenylporphyrin and its dication. *Spectrochim Acta A Mol Biomol Spectrosc* 61:3070–3076.
- Shimanouchi, T. (1972) *Tables of Molecular Vibrational Frequencies*, consolidated Vol. 1, National Bureau of Standards, Washington, DC, pp 1–160.
- Suo, Z., Avci, R., Schweitzer, M.H., and Deliorman, M. (2007) Porphyrin as an ideal biomarker in the search for extraterrestrial life. *Astrobiology* 7:605–615.
- Vidal-Madjar, A. (1975) Evolution of the solar Lyman alpha flux during four consecutive years. *Solar Physics* 40: 69–86.
- Wayland, B.B. and Olson, L.W. (1974) Spectroscopic studies and bonding model for nitric oxide complexes of iron porphyrins. *J Am Chem Soc* 96:6037–6041.
- Wayland, B.B., Mehne, L.F., and Swartz, J. (1978) Mono- and biscarbonyl complexes of iron(II) tetraphenylporphyrin. *J Am Chem Soc* 100:2379–2383.
- Weinkauf, J.R., Cooper, S.W., Schweiger, A., and Wamser, C.C. (2003) Substituent and solvent effects on the hyperporphyrin spectra of diprotonated tetraphenylporphyrins. *J Phys Chem A* 107:3486–3496.

Address correspondence to:  
Amanda M. Cook  
NASA Ames Research Center  
M.S. 245-3  
Moffett Field, CA 94035-1000

E-mail: amanda.m.cook@nasa.gov

Submitted 11 March 2013  
Accepted 27 October 2013